Galactic structure towards the open clusters NGC 188 and NGC 3680

R. A. Méndez Yale University Observatory and European Southern Observatory

> W. F. van Altena Yale University Observatory

Received 1995 December 15; accepted 26 April 1996

To appear in The Astronomical Journal, August 1996 issue

ABSTRACT

We present the first comparisons of a newly developed Galactic Structure and Kinematic Model to magnitude and color counts, as well as relative proper motions, in the fields of the open clusters NGC 188 $((l,b) = (122.8^{\circ}, +22.4^{\circ}))$ and NGC 3680 $((l,b) = (286.8^{\circ}, +16.9^{\circ}))$. In addition to determining the reddening toward these two clusters, it is shown that starcounts at intermediate Galactic latitudes in the range $11 \le V \le 17$ allow us to constrain the model scale-height for disk subgiants. We obtain a mean value of 250 ± 32 pc, in agreement with previous determinations of the scale-height for red-quants. We are also able to constrain the scale-height of main-sequence stars, and the distance of the sun from the Galactic plane, ruling out the possibility of a value of +40pc, in favor of a smaller value. Comparisons with the observed proper-motion histograms indicate that the velocity dispersion of disk main-sequence stars must increase with distance from the Galactic plane in order to match the observed proper-motion dispersion. The required increase is consistent with the values predicted by dynamical models, and provides a clear observational evidence in favor of such gradients. The shape of the observed proper-motion distribution is well fitted within the Poisson uncertainties. This implies that corrections to absolute proper motion (and, therefore, space velocities) for open clusters may be obtained using our model when no inertial reference frame is available. Using this approach, the derived tangential motions for NGC 188 and NGC 3680 are presented.

 $Subject\ headings:$ Galaxy: starcounts — kinematics: proper motions — open clusters: tangential motions

1. Introduction

The use of starcount models to constrain global Galactic Structure parameters has proved to be an effective way of investigating the broad properties of stellar populations in our Galaxy (Reid and Majewski 1993 and references therein). However, most of the proposed models have lacked the ability to predict starcounts and kinematics simultaneously, with a few notable exceptions (Robin and Oblak 1987, Ratnatunga et al. 1989). Furthermore, models that do predict kinematics have not been extensively used. With the wealth of information related to Galactic Structure and Kinematics that is expected to emerge from the Northern Proper Motion Program (Klemola et al. 1987), and its Southern counterpart, the Southern Proper Motion Program (van Altena et al. 1994), as well as from the ongoing measurement of POSS-II plates (Humphreys 1993), we thought it would be interesting to explore the potentials and limitations of a galactic model that incorporates kinematics, in preparation for the advent of these mammoth photometric and kinematic surveys. An additional motivation is the need for a code to predict secular proper motion (Majewski 1993) and the correction to absolute parallax (Monet 1988) for any position in the sky, and under arbitrary selection constraints. In what follows we present the first comparisons of our model to magnitude and color counts, as well as proper-motion distributions for two surveys in the fields of the Galactic clusters NGC 188 and NGC 3680. In the second section a description of the model is provided. Then, in the third section, a brief description of the data is outlined and the model comparisons to star- and color counts as well as kinematic histograms is presented. Finally, in the fourth section, a brief summary of our findings is given.

2. The model

2.1. The starcounts model

Starcounts are computed by using the so-called fundamental equation of stellar statistics (Trumpler and Weaver 1962, Mihalas and Binney 1981). We have followed a parametrization of the density functions, luminosity functions, and Hess-diagrams, similar to that employed by other recent starcount models (see, e.g., Reid and Majewski 1993). We have considered a three-component model that includes a disk, a thick-disk, and a halo. For our present purposes of comparing to bright, low-latitude counts, the contribution of thick-disk and halo stars is minimal, and can be ignored. We have nevertheless included them for completeness and for future applications of our model. It should be emphasized that in no case are the present comparisons attempts to constrain any of the adopted parameters for the thick-disk and halo, rather we concentrate on the disk, which is the dominant component at least to $V \sim 20$ at the Galactic Poles (Reid and Majewski 1993) and even at fainter magnitudes at low Galactic latitudes. Table 1 summarizes the main parameters adopted in the model. These parameters represent a compromise value between

many determinations, and should be viewed as free parameters to be constrained by our comparisons to different data sets. Our task is to identify which parameters have the most impact on the observables (Section 3.1 and 3.2).

Since the disk is the population targeted in this study, a brief description of the adopted density function, luminosity function, and Hess-diagram is necessary. For our density function we have adopted a double-exponentially decaying layer away from the Galactic center in the radial direction, and away from the Galactic plane in the direction perpendicular to the Galactic plane. Surface photometry of edge-on Spiral galaxies indicates that their radial light profile follows quite closely that of an exponential function decaying away from the nucleus (van der Kruit and Searle 1981). On the other hand, an isothermal, self-gravitating disk exhibits a $sech^2(Z/H_z^s)$ density law perpendicular to the Galactic plane (Spitzer 1942) that approximates an exponential function away from the plane (van der Kruit and Searle 1981), where H_z^s is the corresponding $sech^2$ scale-height (see Equation 6). This has motivated the adoption of various exponential-like functions as a representation of the stellar density profile perpendicular to the Galactic plane for both the disk and thick-disk (Reid and Majewski 1993, von Hippel and Bothun 1993, Robin et al. 1996, Ojha et al. 1996), as well as for individual tracers within these components (e.g., for planetary nebulae Zjilstra and Pottasch 1991, Maciel and Dutra 1992).

The stellar density of the Galactic disk in different absolute magnitude intervals has been obtained by several authors. The latest value, determined from the third edition of the Catalogue of Nearby Stars (CNS3 hereafter, Jahreiss and Gliese 1993), indicates a density of 0.12 $stars/pc^3$, with a formal uncertainty of 10 % (Jahreiss 1993). This number has been determined mainly from the stellar sample closer than 5 pc (66 stars), where small number statistics can dominate over any true fluctuations in the stellar density. The sample might not be complete, for example, if we also add reliable spectroscopic and astrometric binaries, the number of stars within that distance limit increases to 70, which is already a change of 6 % in the stellar density (Jahreiss and Gliese 1993). Other determinations of the stellar density are those of Agekjan and Ogorodnikov (1974) which yield a value of $0.138 \pm 0.009 \ stars/pc^3$ for $-1.0 \le M_v \le 19.5$ from the Catalogue of Nearby Stars by Woolley et al. (1970), while from Wielen et al. (1983), we infer $0.119 \pm 0.012 \ stars/pc^3$ in the magnitude range $-1.5 \le M_v \le 21.5$. Indeed, one might expect this number to have fluctuations as lines of sight cross regions of slightly different stellar density. However, Bahcall (1986) has claimed this value to be constant within 15 % in the range $+5 \le M_v < +13.5$ from a comparison of his model to several (high-latitude) fields. Bahcall's result is, therefore, in agreement with the uncertainty of 10% quoted by Jahreiss and Gliese from the CNS3, and leaves very little room for big stellar density fluctuations in the previously mentioned absolute magnitude range.

For the scale-length of the disk, we have adopted 3.5 kpc, similar to other models of this kind (Gilmore 1984, Colles et al. 1991, Bahcall 1986). It should be noted however that some recent starcounts at low and intermediate Galactic latitudes have lead to discrepant

values; While Robin et al. (1992) and Ojha et al. (1994a,b) found smaller values, in the range $\sim 2.0-2.5$ kpc (similar to the values inferred from infrared starcounts, see Kent et al. 1991 for a review), Yamagata and Yoshii (1992) have found a value closer to 4.0 kpc from starcounts in similar directions, although their counts do not seem to agree with those by Soubiran (1992). We have adopted a variable scale-height for main-sequence stars to account for the known fact that older stars have diffused to larger distances from the Galactic plane than younger stars (Wielen and Fuchs 1983). The functional form described by Miller and Scalo (1979), and Bahcall and Soneira (1980), which seems to be a good representation of the available observational data (see also Gilmore and Reid 1983), has been included in our model in the way indicated by Bahcall (1986). On the other hand, subgiants, giants, and white-dwarfs have been assigned a fixed value for the scale-height (see Table 1). Section 3.2 presents the sensitivity of our model to both the scale-length and scale-height of the disk. We find that starcounts toward our two clusters are not sensitive to the scale-length of the disk. The situation is different with the scale-height: we are able to put significant constraints on this parameter for subgiants and main-sequence stars (see Section 3.2).

Our disk luminosity function is Wielen's et al. (1983) for $M_v > +4$. For $M_v < -1$ Wielen's function becomes increasingly incomplete (with only one star at $M_v = -1$, and 4 stars at $M_v = 0$ within 20 pc of the Sun), and we have adopted instead McCuskey's function (1966) as a better representation in this absolute magnitude range. There is very good agreement in the region of overlap, $-1 \le M_v < +4$, where we have adopted the average of both functions. This procedure is similar to that adopted by Bahcall et al. (1987). Our present comparisons are not sensitive to bright giants and supergiants, but we have included this improved luminosity function for future applications of the model. In addition, the still large uncertainties at the faint end of the luminosity function ($M_v > +10$, Kirkpatrick et al. 1994, Reid et al. 1995), do not affect the present results, which are mainly concerned with stars in the range $+1 < M_v < +5$. Since the disk's luminosity function has been well sampled in this magnitude range, we have assumed it to be fixed and equal to the composite value derived in the way described above.

As for the disk's Hess-diagram, we have adopted Robin and Crézé's (1986) values, with the exception of the range $+2.75 \le M_v < 0.25$ and $(B-V)_o \ge +0.9$ where their diagram excludes some G-type subgiants. In this magnitude range we have used the values derived from the CNS3 (there are some 40 stars in the CNS3 that satisfy the above luminosity and color criteria). The lack of subgiants in Robin and Crézé's Hess-diagram is also indicated by a depression of about a factor of two in their luminosity function when compared to Wielen's et al. (1983) or McCuskey's (1966) in the absolute magnitude range mentioned before. The origin of the discrepancy between the observed density of subgiants in the local neighborhood and that adopted by Robin and Crézé is unclear, but it has been recognized, indirectly, by Robin et al. (1992) when comparing Robin and Crézé's model to low-latitude counts. A detailed description of our method employed to update this region

of the Hess-diagram will be presented elsewhere as it bears minimal implications for the current application of our model.

2.2. The kinematic model

Velocity distributions along the line-of-sight and in the tangential direction are computed self-consistently by using velocity ellipsoids evaluated at each distance shell in the corresponding starcount integration. We have adopted Schwarzschild's velocity ellipsoids (1907, 1908). This velocity distribution has not been derived dynamically, but it provides a good description of the observed velocity distribution for stars in the solar neighborhood (Mihalas and Binney 1981, Ratnatunga et al. 1989). King (1990) has argued that it is reasonable to assume that the velocity distribution takes a similar form elsewhere in the Galaxy. However, it can be shown that Schwarzschild's hypothesis predicts that the velocity dispersion in the radial direction is independent of galactocentric distance (Fricke 1952), contrary to the observations (Lewis and Freeman 1989). On the other hand, equilibrium solutions for low-velocity populations in disk-like orbits can indeed be well approximated by Gaussians (Shu 1969, Villumsen and Binney 1985). Also, as pointed out by King (1990), Schwarzschild's velocity ellipsoids, despite their flaws, lead to solutions that are able to predict many details of Galactic structure and kinematics. Therefore, we have adopted the view that these velocity ellipsoids are a good starting point for the kinematic modeling. In what follows we describe the two main parameters that specify the velocity ellipsoid, namely, velocity dispersions and velocity lags.

First-guess velocity dispersions have been taken from the literature. Ratnatunga et al. (1989) have compiled results obtained by Delhaye (1965). These values coincide approximately with the compilation presented by Mihalas and Binney (1981), also derived from Delhaye's values. In addition, Ratnatunga et al. (1989) have derived a set of velocity dispersions from a maximum likelihood analysis of the Bright Star Catalogue (BSC hereafter, Hoffleit 1982), using the observed radial velocities, exclusively. We have adopted a variation of the velocity dispersions with spectral type and luminosity class similar to that of Ratnatunga et al. Our adopted velocity dispersions are shown in Table 2. The velocity dispersions listed in Table 2 are of course the *local* values appropriate for the solar neighborhood. Unfortunately, there is very limited information available on the *change* of velocity dispersion as a function of position in the Galaxy (this is, of course, one of the motivations for the present model). The only evidence comes from the study of K giants by Lewis and Freeman (1989). They found that the component of velocity dispersion along the radial direction (in a cylindrical coordinate system) follows a decaying exponential function away from the Galactic center, with a scale-length similar to that of the disk. They also found that the V-component of the velocity dispersion (along Galactic rotation) followed a similar trend, but with a different scale-height, indicative of a non-flat rotation curve. In our model, we have adopted this functional form for the U-velocity dispersion, while the

V-velocity dispersion has been assumed to follow from the collisionless Boltzmann equation (CBE hereafter, Binney and Tremaine 1987). As for the vertical velocity dispersion, Σ_w , dynamical balance requirements as well as observations of disks in external galaxies (Binney and Tremaine 1987) suggest that Σ_w should be proportional to the stellar (surface) density. All these assumptions lead to the following functional variation for our *model* velocity dispersions:

$$\Sigma_u^2(R) = \Sigma_u^2 e^{-\frac{(R-R_o)}{H_R}} \tag{1}$$

$$\Sigma_v^2(R) = \frac{1}{2} \left(1 + \frac{dlnV_c(R)}{dlnR} \right) \Sigma_u^2(R)$$
 (2)

$$\Sigma_w^2(R) = \Sigma_w^2 e^{-\frac{(R-R_o)}{H_R}} \tag{3}$$

where R_o is the Solar galactocentric distance, H_R is the disk scale-length, Σ_u and Σ_w are the local velocity dispersion in U and W respectively, and $V_c(R)$ is the circular speed (i.e., the rotation curve or, equivalently, the motion of the Local Standard of Rest) at distance R from the Galactic center (assumed to have a local value of 220 km/s). The Z-dependence on $\Sigma_w^2(R)$ has been removed by the vertical integration of our adopted density law. Indeed, it seems that the vertical gradient of the W-velocity dispersion is rather small (Fuchs and Wielen 1987), or zero (Sommer-Larsen 1991). We have started by assuming this gradient to be zero for all three components of the velocity dispersion (Antonuccio-Delogu 1991), but see Section 3.3.

The velocity ellipsoids are computed with respect to the mean speed of the particular Galactic component being evaluated. Since, for an equilibrium system, less rotational support is needed for higher velocity dispersion stars (the so-called asymmetric drift), we have evaluated the mean speed from a self-consistent solution to the CBE (Binney and Tremaine 1987). For a steady-state disk that is not expanding nor contracting, the mean rotational speed, $\langle V(R,Z) \rangle$, is given by

$$< V(R,Z) > = \sqrt{V_c^2(R) - \Sigma_v^2(R) + \left(1 - \frac{2R}{H_R} + S(R,Z)\right) \Sigma_u^2(R)}$$
 (4)

where S(R,Z) is a function that describes the contribution to the rotational support from the cross term Σ_{uv} (usually referred to as the tilt of the velocity ellipsoid). It can be shown that the function S(R,Z) is given by

$$S(R,Z) = q \frac{(\lambda^2 - 1)R^2}{(R^2 + \lambda^2 Z^2)\lambda^2} \left(\frac{(R^2 - \lambda^2 Z^2)}{(R^2 + \lambda^2 Z^2)} - \frac{|Z|}{H_Z} \right)$$
 (5)

where q is zero if the velocity ellipsoid has cylindrical symmetry, or one if the velocity ellipsoid has spherical symmetry, λ is the (fixed) aspect ratio of the velocity ellipsoid, defined by Σ_u/Σ_w , evaluated at Z= 0, and H_z is the exponential scale-height for the population considered. Equation (5) has been obtained by using the expression for Σ_{uv} presented by Kuijken and Gilmore (1989a). The value for λ is in the range 1.5 to 2 for disk stars, e.g., Gilmore et al. (1989) adopted $\lambda = 1.95$ for K and M dwarfs (see also Antonuccio-Delogu 1991), in close agreement with our adopted value of $\lambda = 2.0$ for dwarfs fainter than $M_v = +4.8$ (Table 2). The velocity lags computed from Equation (4) are consistent with the values derived by Ratnatunga et al. (1989) from their analysis of the BSC, as well as with those adopted by Robin and Oblak (1987) in their kinematic model.

3. The Data and Comparison to the Model

3.1. Overview

We have selected two recent photometric and proper-motion surveys to carry out our model comparisons. These are surveys in the fields of the open clusters NGC 188 (Dinescu et al. 1996) and NGC 3680 (Kozhurina-Platais et al. 1995) whose main objective was to provide membership probabilities. The scope and accuracy of both surveys is quite similar, and are described in the respective papers. The existence of clusters in the field of view makes an analysis of the field stars more complex. However, we gain from the astrometric point of view by having a good reference frame (the cluster stars themselves) from which it is possible to calibrate systematic effects (e.g., magnitude equation) that would otherwise limit the accuracy of proper motions for field stars. In addition, these data sets provide an opportunity to examine the possibility of using our model for correcting relative to absolute proper motions (including secular proper motion) by matching the *shape* of the observed proper-motion distribution to that predicted by our model.

Completeness limits, areal coverage, and number of stars included in each survey are shown in Table 3. The bright-magnitude limit was imposed by the constraint of having good S/N (assumed to be Poisson-dominated) on the brightest magnitude bins and also by having enough cluster members to be able to constrain the magnitude equation on the plates utilized. The number of field stars has been computed by using the membership probabilities provided in the individual studies. These memberships were computed using proper motion alone, and proper motion and spatial probabilities combined. We have adopted the latter, although the difference in the total counts by using either method is not significant (see Table 3).

We have performed completeness tests on both samples by using a modified version of the test presented by Bienaymé et al. (1992). Our nearest-neighbor test gives the number of stars with closest neighbor at distances equal to or larger than a given distance.

For a uniform distribution of stars (such as that expected in our field, in the absence of the clusters), the distribution follows an exponentially decaying function with the square of the distance. At shorter distances the expected and observed functions should differ, because of images lost by crowding. The difference between the two functions evaluated at zero distance (i.e., including stars at all separations) gives the absolute completeness of the sample. The absolute completeness is evaluated by fitting the expected distribution to the observed one at large distances, where crowding losses do not occur. Our test is more stable than that used by Bienaymé et al. (1992), since the absolute completeness is calibrated in the regime where losses are not expected (this regime has been adopted as the distance larger than or equal to the distance at which the expected cumulative distribution is independent of the stellar density, equivalent to about 100 arc-sec in the NGC 188 field and to about 50 arc-sec in the NGC 3680 field). Figure 1 shows the best χ^2 model fits to the observed distributions. In order to take into account the presence of the clusters, membership probabilities have been used to compute the cumulative numbers. In addition, to take into account the fact that we may be searching for the nearest star to a cluster star, we have excluded all those stars that exceed a certain threshold probability. This threshold probability has been computed so that the total number of excluded stars equals the number of cluster stars in the field, as deduced from the membership probabilities. For NGC 188 we seem to have more stars at smaller separations than expected. This could be due to some remaining contamination from the cluster which is difficult to separate from the field, especially at the fainter magnitudes of the survey. The extant contamination amounts to, at most, 17 % of the total field star sample. This number is perhaps an overestimation, because it will imply that about 50% of the *cluster* sample would be missing, which is rather larger considering the proper-motion errors quoted by Dinescu et al. (1995). For NGC 3680, we obtain a much better fit, indicating an incompleteness of 4 to 5\%. Since both samples will be binned, the quoted incompleteness for NGC 3680, and the possible cluster contamination in the field of NGC 188, does not alter our conclusions in any significant way.

3.2. Magnitude and Color counts

Figure 2 shows the observed vs. predicted field star magnitude counts for the fields of NGC 188 and NGC 3680. Figure 3 shows the color histograms. In all histograms, the observed values represent sums over the complement of the combined proper-motion and spatial membership probabilities. The parameters adopted for these runs are those indicated in Table 1. We have taken approximate reddening values towards these two clusters from the literature. The overall fit to both the color and magnitude counts for NGC 3680 is remarkable. For NGC 188 the shape of the histograms is similar, but the observed number of stars is larger than expected. This we assume to be due to a larger space density toward this particular line-of-sight, the derived value being $0.17 \pm 0.01 stars/pc^3$. This higher value is unlikely to be due entirely to cluster contamination which, as we have seen, amounts

to less than 17%, whereas the observed over-density is around 44%. Also, the overdensity does not seem to be a strong function of magnitude, which would be the case if cluster contamination were its cause. In what follows we have scaled all our model computations assuming this over-density in the field of NGC 188, while no scaling has been applied to the model for the NGC 3680 field.

We have explored the sensitivity of our model predictions to a number of parameters. For the most sensitive parameters, we have adopted an iterative scheme that allows us to obtain the best overall χ^2 fit to the observed magnitude and color counts simultaneously, while keeping the least significant parameters fixed to their adopted values. In the magnitude range of our surveys, the color counts (once convolved with our photometric errors of $\sim 0.1 \, mag$ in B-V) do not present any strong signature as a function of magnitude (see also Fig 2b on Lasker et al. 1987, and Figure 6 on Ojha et al. 1994c). Therefore, given the small sample size (particularly in the case of the NGC 188 field), we have performed our comparisons to the overall color distribution in the magnitude range where each survey is complete (Table 3), rather than breaking the color counts on different magnitude intervals. Larger samples with smaller photometric errors ($\leq 0.02 \, mag$ in B-V) would be required to cleanly separate field main-sequence from subgiant/giant stars. Nevertheless, we have performed some comparisons to our sample broken down by magnitude and have found that the errors derived for our model parameters (see next paragraph) from our global minimization scheme are kept to a minimum if we use the complete samples, rather than breaking them into smaller sub-samples according to apparent magnitude or color (this is also true for our kinematic modeling, see Section 3.3.)

We find that our model's predictions are not sensitive to the adopted values for the Solar-galactocentric distance (R_{\odot}) or the scale-length (H_R) . This is explained by the fact that the galactic position of our two fields ($l \sim 123^{\circ}$ for the NGC 188 field, $l \sim 287^{\circ}$ for the NGC 3680 field) is such that only a small range in galactocentric distance is included in the starcounts. For example, at 2 kpc (maximum typical distance for faintest stars on both surveys), the galactocentric distance turns out to be 9.6 kpc in the NGC 188 field and 8.2 kpc in the NGC 3680 field. Evidently, fields on the meridional plane of the Galaxy ($l \sim 0^{\circ}$ and $l \sim 180^{\circ}$) would be more appropriate to attempt to constrain R_{\odot} and H_R , as indeed has been done by Robin et al. (1992) and Ojha et al. (1994a,b). For those parameters that turn out to be sensitive, we present in Table 4 their derived values and uncertainties (at the 99% confidence interval (CI), or, equivalently, 3σ , using the parameter estimation scheme described by Lampton et al. 1976). Not surprisingly, the adopted reddening is an important parameter that affects both the total number of field stars as well as the color distribution. More interestingly, we have found that starcounts at intermediate latitudes such as these allow us to constrain directly the scale-height for subgiants $(M_v < +3.0, (B-V)_o > 0.6)$, despite previous claims that only bright (V < 10), all-sky, starcounts could reliably constrain this parameter (McLaughlin 1983, Bahcall 1986).

It should be stated that, since there is a wide age-span in the Disk for stars which

have just left the main-sequence (\sim Hyades age at $M_v = +1$ to \sim M67 age at $M_v = +3$, see notes to Table 2), our derived scale-height has to be seen as a weighted mean value, involving the star formation rate in the disk, and the surface density of matter (see, e.g., Equations (9) and (11) in van der Kruit and Searle 1982, or Equation (16) in Rohlfs and Wiemer 1982). In the case of giants, van der Kruit and Searle 1982 have shown that, for a velocity-independent diffusion coefficient (Wielen 1977), their scale-height would be constant, independent of the details of the star formation history, which simplifies the interpretation of a single scale-height for this population. For subgiants, the situation is more complicated, indeed main-sequence stars in the same absolute magnitude range exhibit a rapid change of scale-height with M_v (see next paragraph). However, it is interesting to notice that our single-number parametrization yields a scale-height which is also consistent with that for giants. In the case of a velocity-dependent coefficient (Wielen and Fuchs 1983, their Equation (27)), the change with time of the scale-height would be less than 5% in the age-interval of disk subgiants, this change would be negligible in comparison with our statistical uncertainties (see Table 4). As an extreme case, we have run a model with a scale-height for subgiants similar to that of main-sequence stars of the same luminosity. The results are shown in Figures 4 and 5 for the magnitude and color counts respectively. This assumption about the scale-height provides a somewhat worse fit to the magnitude counts, and the discrepancies become more evident in the color histograms. However, larger samples are clearly desirable to settle this point.

We have also tested the sensitivity of our derived parameters, to the form of the density function away from the Galactic plane. For this purpose we have considered a $sech^2(Z/H_z^s)$ function. Continuity of the density and its first derivative at large densities from the plane (where observations indicate an exponential decay in stellar density for disk objects) require that

$$H_z^s = 2 \times H_z \tag{6}$$

$$H_z^s = 2 \times H_z \tag{6}$$

$$\rho^s(0) = \frac{\rho(0)}{4} \tag{7}$$

where $\rho^s(0)$ and $\rho(0)$ are the densities, at the plane, for the $sech^2$ and the exponential representations respectively.

Figures 4 and 5 indicate the results of our runs, adopting the values for H_z (Table 4) and $\rho(0)$ from our Hess-diagram (see Section 2.1). It can be seen that these particular counts are not sensitive to our adopted density function, and that, moreover, continuity at large distances form the plane does provide a meaningful constraint to explore other plausible density laws on larger samples.

We are also able to set the overall level for the scale-height of main-sequence stars $(H_Z(MS))$ in the range $+2 \leq M_v \leq +4$, where the scale-height changes very quickly with M_v . The compilations by Miller and Scalo (1979) and Bahcall and Soneira (1980), as well as the results from Gilmore and Reid (1983), seem to indicate that the scale-height for main-sequence stars is approximately constant for $M_v \leq +2$ ($\sim 90~pc$) and for $M_v > +5$ ($\sim 325~pc$). Following Bahcall (1986), we have used a linear interpolation between $M_v = +2$ and $M_v = +5$. We have considered two extreme cases, taken from the range allowed by observational data (Gilmore and Reid 1983), by assuming a "lower" envelope and an "upper" envelope for $H_Z(MS)$. The lower envelope is described by a scale-height of 50 pc for early type stars and 300 pc for later type stars, the upper envelope is described by a scale-height of 120 pc for early type stars and 400 pc for later type stars. The upper and lower envelopes are self-similar, in that the slope of the linear interpolation for $H_Z(MS)$ between the early and late type stars was kept constant at the same value adopted by Bahcall (1986), namely, $\sim 84~pc/M_v$. The implied values for the scale-height of early and late type main-sequence stars for both fields is also shown Table 4.

We obtain some marginal sensitivity to the distance of the Sun from the plane, Z_{\odot} . The results in Table 4 show that the 99% confidence interval is extremely wide. We have, therefore, adopted for Z_{\odot} the IAU value (Blaauw et al. 1959), namely +7 pc. We should notice here that Yamagata and Yoshii (1992) have found a value close to +40 pc for Z_{\odot} from an analysis of starcount data near the north and south galactic poles. It seems, however, that taking the results for NGC 188 and NGC 3680 together, a value as high as +40 pc is ruled-out by our model.

3.3. Proper Motions

The kinematic comparisons take the form of histograms of proper motions in galactic longitude (μ_l) and galactic latitude (μ_b) . Both the observed and the model histograms are fully convolved with observational errors, so that the comparisons can be carried out directly. The parameters derived from the magnitude and color counts described in the previous section were adopted for all the runs described here. Rather than making the comparisons graphically, we have looked at statistical descriptors of the proper-motion distribution; the median proper motion and the proper-motion dispersion (however, the full shape of the proper-motion histograms will be used later on for an assessment of the overall fit to our model predictions). In order to properly handle outliers, these parameters were determined from the observed histograms in an iterative way: Preliminary values for the median and dispersion were computed, then a window of semi-width three times the proper-motion dispersion centered on the median was used to recompute the median and dispersion, until convergence. The derived values for the observed proper-motion dispersion were also adopted as the window on the model histograms. In this case, the iterative procedure was the same as for the observed histogram, except that the window size was kept constant and equal to six-times the observed proper-motion dispersion, centered on the median. We adopted this procedure so that our comparisons encompass exactly the same

proper-motion interval from the median for both the observed and model histograms. This is important in view of the different nature of the extreme outliers on the observed (large errors) and model (velocity ellipsoid wings) histograms. Therefore, it should be understood that the model proper-motion dispersions derived here are the values that one would expect if motions only in the specified proper-motion window are considered.

Figures 6 and 7 show the proper-motion histograms in the field of NGC 188 and NGC 3680 respectively. For these runs, the standard parameters described in Section 2.2 were used. There is relatively good overall agreement between the observed and predicted histograms. The zero-point shift in the histograms is expected, and is due to the fact that we only have proper motions relative to the cluster stars (which have been used to define the reference frame). Therefore, in principle, we can not use these data to test the reliability of our predicted proper-motion zero-point. We can, however, let the zero-point be a free parameter, and compare the shape of the observed vs. predicted histograms. A good match to the shape will indicate that our model assumptions are appropriate. Even though the histograms are not completely symmetric (due to the superposition of velocity ellipsoids with different velocity lags), we have concentrated mainly on the proper-motion dispersion as a diagnostic of our model fits. As for the case of the magnitude and color counts, we have made a number of runs changing the relevant kinematic parameters successively in order to investigate their effect upon the predicted median proper motion and the proper-motion dispersion. Table 5 indicates the observed proper-motion dispersions for these runs as well as their median values. As a general conclusion from these runs one could say that these particular data are unable to discriminate between a velocity ellipsoid oriented toward the Galactic axis of rotation from one oriented towards the Galactic center (q=0 and q=1respectively in Equation (5), Runs 1 and 2 in Table 5). In addition, the overall rotation of the disk does not change the predicted velocity dispersion in a significant way (Runs 3 and 4), a result expected since most stars in these samples are disk stars which are moving with almost the same relative speed. A change of the solar motion affects also mainly the median proper motion, but not the proper-motion dispersion (Run 5). Still, the change is quite small, at most 0.6 mas/yr in μ_l for the NGC 188 field. We have also tried changing the slope of the local rotation curve, to cover the range of present observational uncertainties, between $dV_c(R)/dR \sim -15 \, km/s/kpc$ to $dV_c(R)/dR \sim +5 \, km/s/kpc$ (Kerr and Lynden-Bell 1986). Again, only a small change is seen (Runs 6 and 7).

A common feature that emerges from the runs described above is that the observed and predicted proper-motion dispersions differ by more than the observational error of the former. The discrepancy is larger in the proper-motion dispersion in longitude Σ_{μ_l} than in latitude Σ_{μ_b} . Also, the discrepancy is larger in the NGC 3680 field than in the NGC 188 field, where the difference between the observed and expected dispersions reaches 8σ of the observed uncertainty. In all cases, the observed dispersion is larger that the predicted one. Since the observed proper-motion dispersion is independent of their relative nature, we can attempt to constrain it by comparing to our model predictions directly. Evidently,

the most direct way of increasing the predicted dispersion is to increase either the adopted proper-motion errors (which are included in the error-convolved predicted values) or to increase the model velocity dispersion. In the latter case, the model would allow us to put constraints on the velocity dispersion for those stars that are mostly represented in our sample. We have therefore run models with larger errors than those quoted in Dinescu et al. (1996) and Kozhurina-Platais et al. (1995), and also with increasingly higher velocity dispersions than those given in Table 2. It should be emphasized that our adopted velocity dispersion values have been taken from the compilation by Mihalas and Binney (1981) and from Ratnatunga et al. (1989). The latter quote uncertainties of, at most, 10% for their derived velocity dispersions. We have verified with the model that changes in the adopted velocity dispersion for giants and subgiants cause a negligible change in the proper-motion dispersion (being bright, their mean distance is larger than for the fainter stars, and thus they contribute mainly to the peak of the proper-motion distribution, while nearby main-sequence stars would contribute mainly to the proper-motion wings, i.e., they define the proper-motion dispersion).

Table 5 shows the effect of increasing the quoted errors by 1σ of their uncertainty (Run 8). As it can be seen, the dispersion around the mean proper-motion error (which is a function of apparent magnitude) is small enough that the effect upon the expected values is minimal. In Runs 9 to 11 we indicate, on the other hand, the effect of increasing the velocity dispersion for main-sequence stars by 10, 20, and 30% respectively. In the field of NGC 188 it seems that an increase close to 20% would suffice to fit the observed dispersion in Galactic latitude, and a 30% increase to fit the dispersion along Galactic longitude. In the field of NGC 3680 it seems that an increase larger than 30% would be required to fit either dispersion. These velocity dispersion increases seem uncomfortably large considering the relatively small errors for these values quoted by Ratnatunga et al. (1989), as well as judging from the agreement between different compilations (Delhaye 1965, Mihalas and Binney 1981). Also, it does not seem possible to fit, simultaneously, the dispersion in both coordinates and for both lines-of-sight by merely scaling up the local velocity dispersions. This has prompted us to explore a more interesting dynamical possibility: Fuchs and Wielen (1987) have computed models for the change of velocity dispersion as a function of distance from the Galactic plane under reasonable gravitational potentials. They find that the velocity dispersion in all three coordinates must increase with distance from the plane, in a way almost independent of the assumed potential. We have incorporated their results in our model, by introducing a linear increase of velocity dispersion with distance from the plane. Our adopted values for the slope of the velocity dispersion with |Z|, taken from Fuchs and Wielen (their Figure 4) are given in Table 6. The results of our runs with this modified functional form for the velocity dispersion, but retaining the original local velocity dispersions, are also shown in Table 5 Run 12). We can see a drastic improvement in the agreement between the observed and predicted proper-motion dispersions. The effect of a further 10% increase on the local velocity dispersions for main-sequence stars (allowed by the observational uncertainties in these velocity dispersions) is also indicated in Table 6

(Run 13). This last run provides a better fit to the NGC 3680 data and a somewhat worse fit to the NGC 188 data than does Run 12. We conclude therefore that our data shows a clear indication for an increase of velocity dispersion with distance from the Galactic plane for disk stars in a way similar to that predicted by the dynamical models of Fuchs and Wielen (1987). Kuijken and Gilmore (1989b) have found a similar trend of increasing Σ_w with distance from the Galactic plane from a sample of K dwarfs at the South Galactic Pole. In this case, radial velocities could prove only one velocity direction, while, given the Galactic location of our fields, our proper motions are able to prove, simultaneously, the trend in Σ_u and Σ_w . The inferred value for $d\Sigma_w/dZ$ from Kuijken and Gilmore (1989b, their Figure 13) is 0.0125 km/s/pc in the distance range $|Z| < 1 \, kpc$, quite close to our adopted value from Fuchs and Wielen (1987, see Table 6).

In comparing our expected proper-motion distribution to the observed histogram, there is always the possibility that our velocity distribution does not provide a good description of the underlying distribution. Wielen and Fuchs (1983) have shown that the solution of the Boltzmann equation, including a constant diffusion term, leads, indeed, to a Schwarzschild distribution for a single generation of stars, where the velocity dispersions increase with age. Assuming a constant star formation rate, they have evaluated (Fuchs and Wielen 1987) the resulting velocity distribution function. They find that the implied function has a more pronounced peak and more important outer wings than a Gaussian with the same overall dispersion. This is the natural result of the superposition of several Schwarzschild-type distributions with different velocity dispersion. In a recent study, Reid et al. (1995) have analyzed the kinematics of nearby M dwarfs in the range $8 < M_v < 15$. They find that the overall velocity distribution of these stars can be quite complex (their Figure 11). However, they also find that the velocity distribution for the brighter sample (8 $< M_v <$ 10, their Figure 14) is well reproduced by Gaussians (as discussed by Reid et al., their fainter sample with $M_v > 12$ may be subject to a proper-motion bias). Therefore, for our initial models we have adopted the view that, when properly binned in luminosity (i.e., mean age), the velocity distribution of disk stars is well represented by a Gaussian function as shown by the available observations, and as predicted by the theory of stellar diffusion. Of course, the asymmetric drift will distort these Gaussian functions, but this effect is fully included in the model (Equations 4 and 5).

In our model, we have modeled the change of velocity dispersion with age, as a change of velocity dispersion with absolute magnitude (Table 2). In the following paragraph we show that we are indeed able to reproduce the *shape* of the observed proper-motion distribution within the Poisson noise of our sample, thus providing support to the correctness of our kinematical assumptions at least at the level permitted by the current comparisons. This implies that small local fluctuations in the velocity ellipsoids (due, e.g., to moving groups) which could make a significant contribution at larger distances from the plane are not present in the two fields-of-view analyzed here.

As we have pointed out, our motions do not allow us to constrain our model's absolute

proper motions. However, we can still test the overall fit to the observed proper-motion histogram by using the best-fit model obtained above. We have implemented a χ^2 procedure to compute the offset between the observed and predicted proper-motion histograms. Figures 8 and 9 shows the best χ^2 fit to the observed histogram, using Run 13 (Table 5). The uncertainty in the proper-motion offsets at the 1σ level is indicated in the first two rows on Table 7. From this table we see that our 1σ uncertainties in the zero-point correction are *similar* to the uncertainties in the observed median proper motion (Table 5), which is determined by the width of the proper motion distribution (determined by nature) and the sample size (determined by the observer). This implies that our fits, for these two samples, are limited not by our ability to model the observed proper-motion histograms correctly but, rather, by the noise in the observed histograms themselves. Evidently, a systematic error in our adopted distances or velocities would be reflected not only by an offset in the computed proper motion, but also by the shape of the proper motion distribution, which will lead to an uncertainty of our fits larger than the uncertainty in the median, contrary to our findings. This opens the prospect for using our model to correct the relative proper motions for cluster stars in these two studies to an absolute reference frame, allowing us to derive their space velocities. Since the motion of the field stars relative to the cluster is the same regardless of what reference frame is used, we have the basic constraint

$$\vec{\mu}_{cl}^a - \vec{\mu}_f^a = \vec{\mu}_{cl}^r - \vec{\mu}_f^r \tag{8}$$

where the superindices refer to absolute (a) and relative (r) proper motion, and the subindices refer to cluster (cl) and field (f). In proper-motion based membership studies it is customary to use the cluster stars themselves as the reference frame, due to their smaller intrinsic proper-motion dispersion. In this case one would have $\vec{\mu}_{cl}^r = \vec{0}$, and therefore the difference $\vec{\mu}_f^a - \vec{\mu}_f^r$ is precisely the absolute motion of the cluster. This difference is the number whose uncertainty we have presented in Table 7. In practice, however, a small residual motion of the cluster is obtained due to the difficulty of selecting, a priori, only cluster members, so that contamination by field stars pulls the motion of the cluster to values different than zero (see e.g. Table 5 in Kozhurina-Platais et al. (1995) or Table 4 in Dinescu et al. (1996)). For this reason, the absolute motion of the cluster would be given by $\vec{\mu}_{cl}^a = \vec{\mu}_f^a + (\vec{\mu}_{cl}^r - \vec{\mu}_f^r)$, where the term in parentheses is taken directly from the respective proper-motion studies, and the absolute motion of the field is computed using our model. The uncertainty of the correction is the propagated error of the correction derived from $\vec{\mu}_f^a - \vec{\mu}_f^r$ (which, as we have seen, is essentially the uncertainty with which one can determine the mean motion of the field stars, and decreases with the field sample size) plus the error in separating cluster from field stars. By using the values for the absolute motion of the field stars quoted in Table 15 (Run 13), and the relative motion of the cluster relative to field stars quoted by Dinescu et al. (1996) for NGC 188 and by Kozhurina-Platais et al. (1995) for NGC 3680, we obtain the absolute motion of both clusters given in Table 7, which also indicates the derived tangential velocities, adopting values for the distance modulus of both clusters from the above papers, indicated in the same table. The final uncertainty in the derived tangential velocities includes only uncertainties in the proper motions and not in the distance modulus, and it is clearly dominated in these two cases by the uncertainty of locating the (relative) median proper motion of field stars rather than the uncertainty of the motion of the cluster relative to the field. Evidently, the best possible test for our model's ability to reproduce the observed median absolute proper motion will come from direct comparisons to absolute proper motions. These comparisons are underway and will be published elsewhere. However, from the relatively small variation of the predicted median proper motion seen in Table 5 for different model assumptions, it is clear that the corrections derived here are likely to be very close to the value we would have derived using an absolute reference frame.

4. Summary

Comparison of our model to observed starcounts toward the open clusters NGC 188 and NGC 3680 are successfully used to constrain several Galactic structure parameters (Table 4). Comparisons to the observed proper motions indicate that the disk shows a velocity dispersion gradient in a way similar to that expected from dynamical models, and for which observational confirmation was awaited (Table 5). In addition, the shape of the observed proper-motion distribution is well matched, and a correction to absolute proper motion for both clusters is derived (Table 7). The velocities obtained for both clusters could be combined with radial velocity studies to yield orbits for NGC 188 and NGC 3680 under suitable gravitational potentials.

Other lines of sight should be investigated to further validate the results presented here. In this context, starcounts and proper motions for field stars in the line-of-sight of intermediate-latitude open clusters (where reddening is not so severe), provide the best opportunity to sample the properties of the Galactic disk (within a radius of 2 kpc or so from the Sun), including the change of kinematical parameters as a function of position in the Galaxy. In addition, the same analysis would yield orbits for those open clusters, from which statistical studies of their orbital parameters and correlations (or lack thereof) with other parameters (e.g., age and metallicity) could be carried out to investigate the dynamical and evolutionary status of the Galactic disk.

I have greatly benefited from conversations with Dr. T. Girard, and Dr. I. Platais, as well as with D. Dinescu and V. Kozhurina-Platais. Several suggestions by Dr. S. Majewski and the anonymous referee(s) have improved the content and scope of this paper. This research has been supported in part by NSF and NASA grants. R. A. M. also acknowledges a travel grant (C-51073) from the Chilean Andes Foundation.

Table 1. Starcounts model parameters

Parameter	Disk	Thick-Disk	Halo
Luminosity Function	McCuskey (1966) & Wielen et al. (1983) ¹	47 Tuc	М 3
Hess-Diagram	Robin and Crézé $(1986)^2$	47 Tuc	M 3
Scale-length	3.5 kpc	$3.5~\mathrm{kpc}$	$2.7 \mathrm{~kpc^3}$
Scale-height	250 pc for giants & subgiants ⁴	$1.4~\mathrm{kpc}$	0.80^{5}
Stellar density	$0.12 stars/pc^3 \text{for} M_v \leq 21.5$		
Local normalizations		2%	0.125%

References. — (1) see text for details; (2) modified to include subgiants from the CNS3; (3) this corresponds to the de Vaucoleurs' half-light radius for an oblate spheroid; (4) 325 pc for white-dwarfs, function of M_v for main-sequence stars, see text for details; (5) axial ratio

Table 2. Model local velocity dispersions

Kinematic group	$\Sigma_u \text{km/s}$	$\frac{\Sigma_v}{\mathrm{km/s}}$	Σ_w km/s
Giants^1	30	20	20
$Sub-giants^2$	30	20	20
Main-sequence			
$M_v \le +2.2$	15	10	10
$+2.2 < M_v \le +4.8$	25	15	15
$+4.8 < M_v$	30	20	15
White-dwarfs	30	20	20

References. — (1) Giants are stars with $M_v \leq -0.7$ and $(B-V)_o > +1.28$, and $-0.7 < M_v \leq +1.0$ and $(B-V)_o > +0.57$; (2) Sub-giants are stars with $+1.0 < M_v \leq +3.0$ and $(B-V)_o > +0.57$

Table 3. Survey characteristics

Parameter	NGC 188 field	NGC 3680 field
Areal coverage	$0.9^{o}X0.8^{o}$	$0.9^{o}X0.6^{o}$
Completeness limit	$12.0 \le V < 15.2$	$11.0 \le V < 16.8$
Total sample ¹	589 stars	1626 stars
Number of field stars		
Using P_{μ} only ²	$430.68 \mathrm{\ stars}$	$1563.83 \mathrm{\ stars}$
Using $P_{\mu,r}$ 3	424.33 stars	$1560.00 \mathrm{\ stars}$
, ,		

References. — (1) within completeness limit; (2) P_{μ} is the membership probability using proper motions exclusively; (3) $P_{\mu,r}$ is the membership probability using both proper motions and spatial distribution of cluster stars.

Table 4. Derived Galactic structure parameters (all quoted uncertainties are 3σ)

Parameter	NGC 188 field	NGC 3680 field
Reddening ¹ $H_z^{(Subgiants)}$ $H_z^{young}(Main - seq)^2$ $H_z^{old}(Main - seq)^2$ Z_{\odot}	$0.067 \pm 0.022 \text{ mag}$ $251 \pm 69 \text{ pc}$ $83 \pm 12 \text{ pc}$ $348 \pm 18 \text{ pc}$ $2 \pm 34 \text{ pc}$	$0.046 \pm 0.017 \text{ mag}$ $249 \pm 38 \text{ pc}$ $78 \pm 8 \text{ pc}$ $340 \pm 11 \text{ pc}$ $-8 \pm 19 \text{ pc}$

References. — (1) value "at infinity", scaled down with an exponential-lab of thickness 100 pc; (2) see text for details

Table 5. Kinematic values for surveys and models

NGC 188 field			NGC 3680 field					
Run	μ_l^m	μ_b^m	σ_{μ_l}	σ_{μ_b}	μ_l^m	μ_b^m	σ_{μ_l}	σ_{μ_b}
Observed	0.47 ± 0.41	1.38 ± 0.26	8.25 ± 0.32	5.10 ± 0.20	-0.23 ± 0.18	-0.08 ± 0.12	7.12 ± 0.14	4.37 ± 0.09
Run 1	1.10	0.35	7.47	4.76	-7.20	-1.57	5.96	3.69
Run 2	1.16	0.37	7.45	4.73	-7.20	-1.60	5.96	3.68
Run 3	1.85	0.27	7.51	4.73	-6.34	-1.68	6.03	3.69
Run 4	0.59	0.49	7.38	4.74	-8.10	-1.55	5.97	3.69
Run 5	0.61	0.42	7.34	4.73	-6.86	-1.47	5.95	3.62
Run 6	0.83	0.22	7.46	4.76	-7.22	-1.65	5.97	3.69
Run 7	2.16	0.82	7.18	4.56	-7.15	-1.43	6.02	3.56
Run 8	1.22	0.36	7.48	4.81	-7.22	-1.62	6.08	3.79
Run 9	1.26	0.46	7.73	4.96	-7.16	-1.64	6.22	3.83
Run 10	1.37	0.58	8.00	5.15	-7.15	-1.66	6.48	3.97
Run 11	1.49	0.69	8.25	5.32	-7.10	-1.70	6.71	4.11
Run 12	2.32	0.90	8.42	5.33	-7.17	-1.90	6.88	4.16
Run 13	2.46	1.04	8.70	5.50	-7.15	-1.93	7.12	4.29

References. — Run 1: Standard values (Table 2), q= 0 (equation (5)); Run2: As Run 1, but q= 1; Run3: $V_c(R)=180\,km/s$; Run4: $V_c(R)=260\,km/s$; Run5: \vec{V}_\odot from Mihalas and Binney (1981) rather than the value obtained by Ratnatunga et al. (1989) used in the previous runs; Run 6: $dV_c(R)/dR \sim +5\,km/s/kpc$; Run 7: $dV_c(R)/dR \sim -15\,km/s/kpc$; Run 8: Errors of proper motion increased by 1σ of their quoted uncertainty; Run 9: 10% increase in main-sequence velocity dispersion; Run 10: 20% increase in main-sequence velocity dispersion; Run 11: 30% increase in main-sequence velocity dispersion; Run 12: Velocity dispersion wth a |Z| gradient as per Fuchs and Wielen (1987); Run 13: As run 12 but, in addition, a 10% increase in main-sequence velocity dispersion

Table 6. Adopted velocity dispersion gradients from the Galactic plane (from Fuchs and Wielen 1987)

Distance from plane pc	$\frac{\frac{d\Sigma_u}{dZ}}{\text{km/s/pc}}$	$\frac{d\Sigma_v}{dZ}$ km/s/pc	$\frac{d\Sigma_w}{dZ}$ km/s/pc
$ Z < 500$ $500 \le Z < 1000$ $1000 \le Z $	$2.72 10^{-2} 9.78 10^{-3} 0.00$	$ \begin{array}{r} 1.74 10^{-2} \\ 5.44 10^{-3} \\ 0.00 \end{array} $	$ \begin{array}{c} 1.41 10^{-2} \\ 5.43 10^{-3} \\ 0.00 \end{array} $

Table 7. Derived tangential motions for the open clusters NGC 188 and NGC 3680

Parameter	NGC 188	NGC 3680
$\sigma_{\Delta\mu_l} \text{ mas/yr}$	± 0.42	±0.19
$\sigma_{\Delta\mu_b}$ mas/yr	± 0.33	± 0.11
$\mu_{l_{cl}}^{a}$ mas/yr	1.17	-7.53
$\mu_{b_{cl}}^{a}$ mas/yr	-0.26	-1.78
m-M mag	11.12	10.00
$V_{l_{cl}} \text{ km/s}$	9.3 ± 3.3	-35.7 ± 0.9
$V_{b_{cl}} \text{ km/s}$	-2.1 ± 2.7	-8.4 ± 0.5

REFERENCES

- Agekjan T. A., and Ogorodnikov, K.F., 1974, in Highlights of Astronomy, Vol. 3, G. Contopoulos, Dordrecht: Reidel, 451
- Antonuccio-Delogu, V., 1991, A&A, 247, 45
- Bahcall, J. N., and Soneira, R. M., 1980, ApJ, 73, 110
- Bahcall, J.N., 1986, Ann. Rev. Astron. and Astrophys., 24, 557
- Bahcall, J. N., Casertano, S., and Ratnatunga, K. U., 1987, AJ, 320, 515
- Bienaymé, O. Mohan, V., Crézé, M., Considerè, S., and Robin, A. C., 1992, A&A, 253, 389
- Binney, J., and Tremaine, S., 1987, Galactic Dynamics, New Jersey: Princeton
- Blaauw, A., Gunn, C. S., Pawsey, J. L., and Westerhout, G., 1959, M. N. R. A. S., 119, 422
- Colles, M., Ellis, R.S., Taylor, K., and Shaw, G., 1991, M.N.R.A.S., 253, 686
- Delhaye, J., 1965, in Galactic Structure, Stars and Stellar Systems, Vol. 5, edited by Adriaan Blaauw and Maarten Schmidt (The University of Chicago, Chicago), page 61
- Dinescu, D. I., Girard, T. M., van Altena, W. F., Yang, T.-G., and Lee, Y.-W., 1996, AJ, 111, 1205
- Fricke, W., 1952, Astr. Nach., 280, 193
- Fuchs, B., and Wielen, R., 1987, The Galaxy, NATO-ASI series, G. Gilmore, B. Carswell, Dordrecht: Reidel, 375
- Gilmore, G., 1984, M.N.R.A.S., 207, 223
- Gilmore, G., and Reid, N., 1983, M.N.R.A.S., 202, 1025
- Gilmore, G., Wyse, R. F. G., and Kuijken, K., 1989, Ann. Rev. Astron. Astrophys., 27, 555
- Hoffleit, D., 1982, The Bright Star Catalogue, 4th ed, New Haven, Yale University Observatory
- Humphreys, R., 1993, Workshop on Databases for Galactic Structure, A. G. Davis Philip, B. Hauck, A. R. Upgren, Schenectady: L. Davis Press, 87
- Jahreiss H., and Gliese W., 1993, Workshop on Databases for Galactic Structure, A. G. Davis Philip, B. Hauck, and A. R. Upgren, Schenectady: L. Davis Press, 53

Jahreiss H., 1993, private communication

Kent, S. M., Dame, T. M., and Fazio, G., 1991, ApJ, 378, 131

Kerr, F. J., and Lynden-Bell, D., 1986, M. N. R. A. S., 221, 1023

King, I. R., 1990, in The Milky Way as a Galaxy, Saas-fee Advanced course No. 19, Roland Buser, Ivan R. King, California: University Science, page 117

Kirkpatrick, J. D., McGraw, J. T., Hess, T. R., Liebert, J., McCarthy, D. W., 1994, Ap. J. Suppl., 94, 749

Klemola, A. R., Jones, B. F., and Hanson, R. B., 1987, AJ, 94, 501

Kozhurina-Platais, V., Girard, T. M., Platais, I., van Altena, W. F., Ianna, P. A., and Cannon, R. D., 1995, AJ, 109, 672

Kuijken, K., and Gilmore, G., 1989a, M.N.R.A.S., 239, 571

Kuijken, K., and Gilmore, G., 1989b, M.N.R.A.S., 239, 605

Lewis, J. R., and Freeman, K. C., 1989, AJ, 97, 139

Lampton, M., Margon, B., and Bowyer S., 1976, ApJ, 208, 177

Lasker, B. M., Garnavich, P. M., and Reynolds, A. P., 1987, ApJ, 320, 502

Maciel, W. J., and Dutra, C. M., 1992, A&A, 262, 271

Majewski, S. R., 1993, Ann. Rev. Astron. Astrophys, 31, 575

McCuskey, S. W., 1966, in Vistas in Astronomy, Vol. 7, A. Beer, Oxford: Pergamon, 141

McLaughlin, S. S., 1983, AJ, 88, 1633

Mihalas, D., and Binney, J., 1981, Galactic Astronomy, New York: Freeman

Miller, G. E., and Scalo, J. M., 1979, ApJ, 41, 513

Monet, D. G., 1988, Ann. Rev. Astron Astrophysics, 26, 413

Ojha, D. K., Bienaymé, O., and Robin, A. C., 1994a, in Astronomy from Wide-Field Imaging, IAU Symposium 161, H. T. MacGillivray, E. B. Thomson, B. M. Lasker, I. N. Reid, D. F. Malin, R. M. West, and H. Lorenz, Dordrecht: Kluwer, 447

Ojha, D. K., Bienaymé, O., Robin, A. C., and Mohan, V., 1994b, A&A, 284, 810

Ojha, D. K., Bienaymé, O., Robin, A. C., and Mohan, V., 1994c, A&A, 290, 771

Ojha, D. K., Bienaymé, O., Robin, A. C., Crézé, M., and Mohan, V., 1996, to appear in A&A

Ratnatunga, K. U., Bahcall, J. N., and Casertano, S., 1989, ApJ, 339, 106

Reid, N., and Majewski, S. R., 1993, ApJ, 409, 635

Reid, I. N., Hawley, S. L., and Gizis, J. E., 1995, AJ, 110, 1838

Robin, A., Crézé, M., 1986, A&A, 151, 71

Robin, A. C., and Oblak, E., 1987, Evolution of Galaxies, 10th IAU European Regional Meeting, Vol. 4, J. Palous, Ondrejov: Astronomical Institute of the Czechoslovak Academy of Sciences, 323

Robin, A.C., Crézé, M., and Mohan, V., 1992, A&A, 265, 32

Robin, A. C., Haywood, M., Crézé, M., Ojha, D. K., and Bienaymé, O., 1996, to appear in A&A

Rohlfs, K., and Wiemer H.-J., 1982, A&A, 112, 116

Schwarzschild, K., 1907, Akad. Wissenschaft Gotingen Nach., 614

Schwarzschild, K., 1908, Akad. Wissenschaft Gotingen Nach., 191

Shu, F., 1969, ApJ, 158, 505

Sommer-Larsen, J., 1991, M.N.R.A.S., 249, 368

Soubiran, C., 1992, A&A, 274, 181

Spitzer, L., 1942, ApJ, 95, 329

Trumpler, R. J., and Weaver, H. F., 1962, Statistical Astronomy, New York: Dover

van Altena, W. F., Platais, I., Girard, T. M., and Lopez, C. E., 1994, in Galactic and Solar System Optical Astrometry, L. V. Morrison and G. F. Gilmore, Cambridge: Cambridge Univ. Press, 26

van der Kruit, P. C., and Searle, L., 1981, A&A, 105, 115

van der Kruit, P. C., and Searle, L., 1982, A&A, 110, 61

Villumsen, J. V., and Binney, J., 1985, ApJ, 295, 388

von Hippel, T., Bothun, G. D., 1993, ApJ, 407, 115

Wielen, R., and Fuchs, B., 1983, in Kinematics, Dynamics, and Structure of the Milky Way, W. L. H. Shuter, Dordrecht: Reidel, 81

Wielen, R., 1977, A&A, 60, 263

Wielen, R., Jahreiss, H., and Kruger, R., 1983, in The nearby stars and the Stellar Luminosity Function, IAU Colloq. 76, A. G. Davis Philip and A. R. Upgren, Schenectady: L. Davis Press, 163

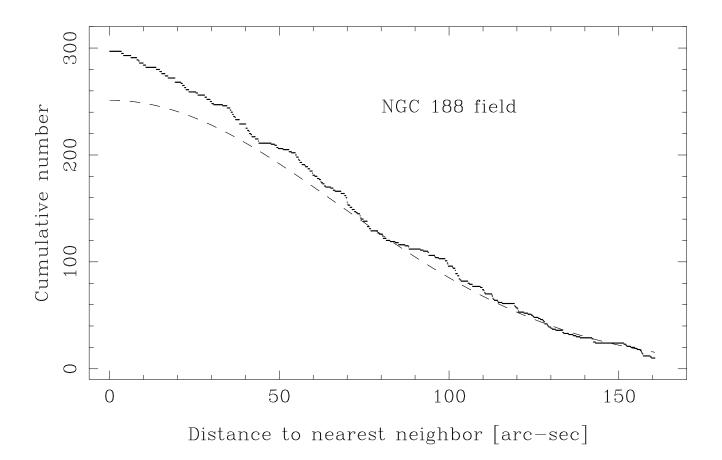
Woolley, R., Epps, E. A., Penston, M. J., and Pocock, B., 1970, Roy. Obs. Ann., 5

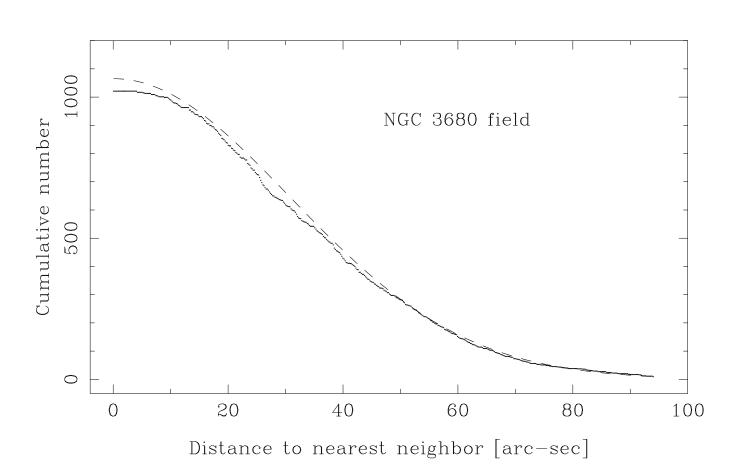
Yamagata, T., and Yoshii, Y., 1992, AJ, 103, 117

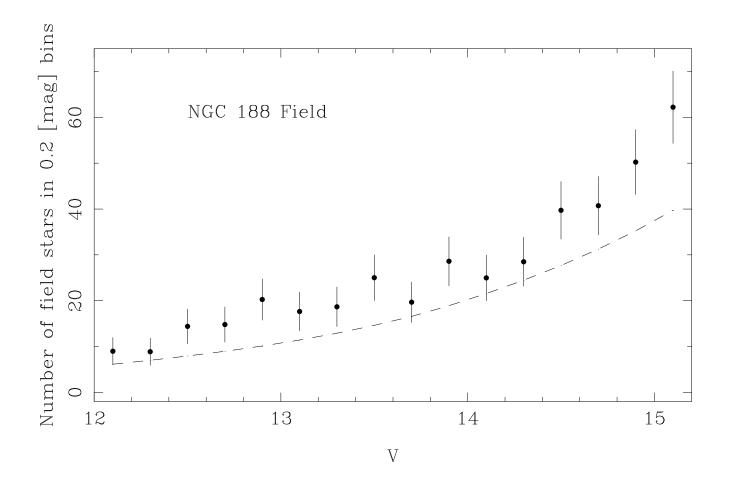
Zjilstra, A. A., and Pottasch, S. R., 1991, A&A, 243, 478

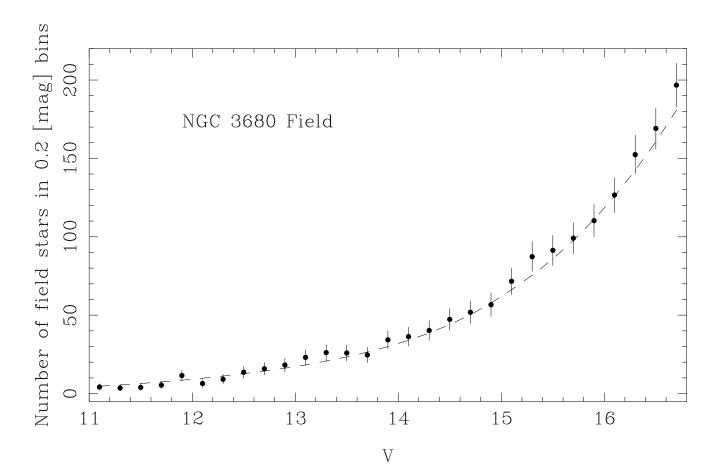
This manuscript was prepared with the AAS IATEX macros v4.0.

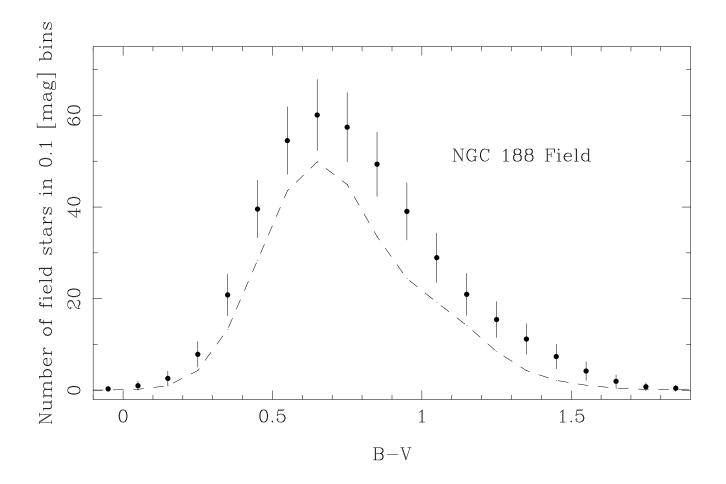
- Fig. 1.— Nearest-neighbor completeness test. Dotted lines represent the data, dashed lines are the best fits to the observed distributions in a range of distances where crowding losses are not expected (100 arc-sec on the NGC 188 field, 50 arc-sec on the NGC 3680 field). The upper panel is for the NGC 188 field, the lower is for the NGC 3680 field.
- Fig. 2.— Starcounts versus apparent V magnitude. Circles and Poisson error bars denote the data, the dashed line is the model. The upper panel is for the NGC 188 field, the lower panel is for the NGC 3680 field.
- Fig. 3.— Color counts versus reddened B-V color within the completeness limits in apparent magnitude specified in Table 3. Symbols as in Figure 2.
- Fig. 4.— Same as Figure 2, except that a different parametrization for the scale-height of subgiants, and a different density law, has been used. The continuous line is the best-fit model (Table 4), the dashed line is the model with a scale-height for subgiants as for main-sequence stars, and the dot-dashed line is the model for a $sech^2$ density law for subgiants.
- Fig. 5.— Same as Figure 3, symbols as in Figure 4. The inadequacy of a scale-height for subgiants similar to that of main-sequence stars is clearly seen in the red wing of the color counts.
- Fig. 6.— Proper-motion histogram of the field of NGC 188 in the magnitude range $12.0 \le V < 15.2$. Symbols as in Figure 2.
- Fig. 7.— Proper-motion histogram of the field of NGC 3680 in the magnitude range $11.0 \le V < 16.8$. Symbols as in Figure 2.
- Fig. 8.— Same as Figure 6, except that the observed data have been shifted in proper motion to best match the predicted distribution. Symbols as in Figure 2.
- Fig. 9.— Same as Figure 7, except that the observed data have been shifted in proper motion to best match the predicted distribution. Symbols as in Figure 2.

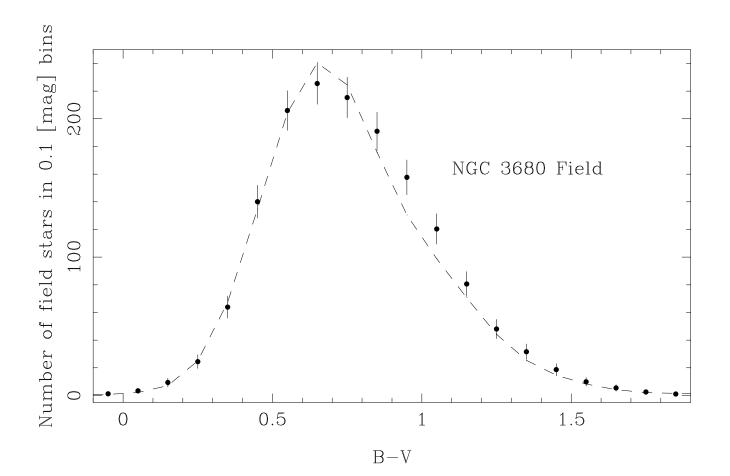


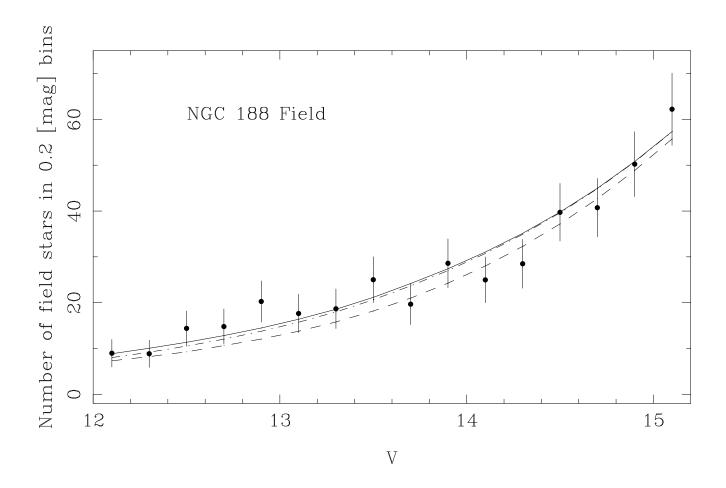


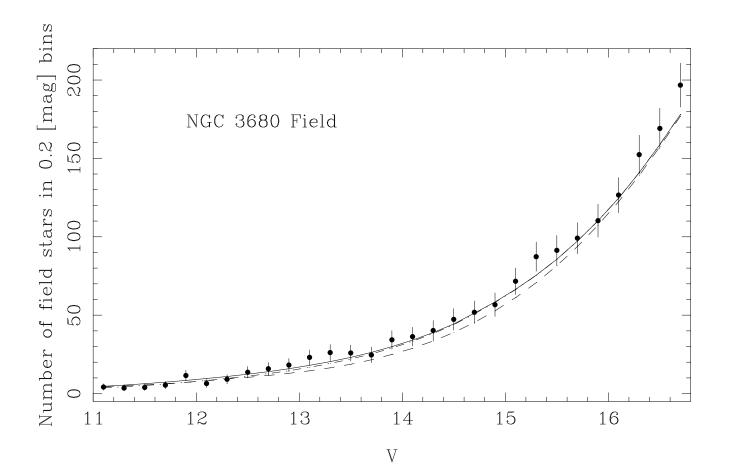


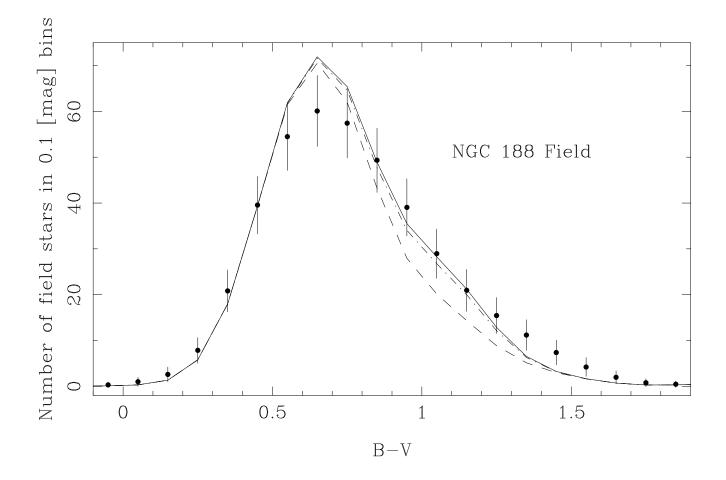


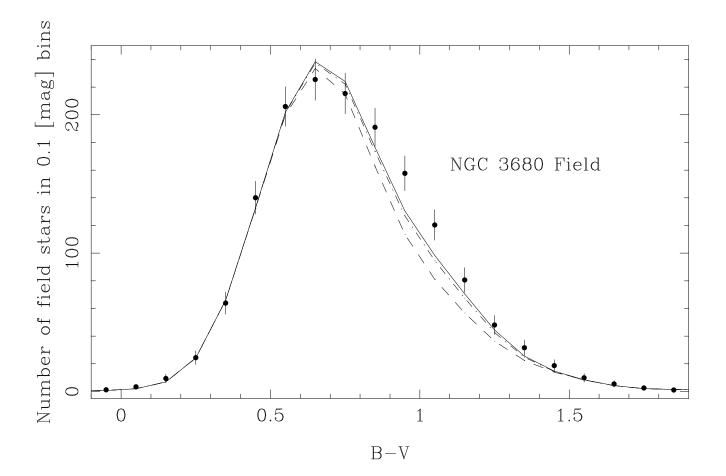


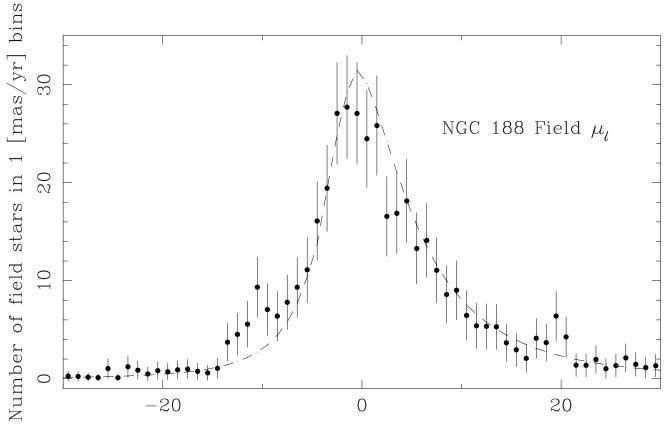




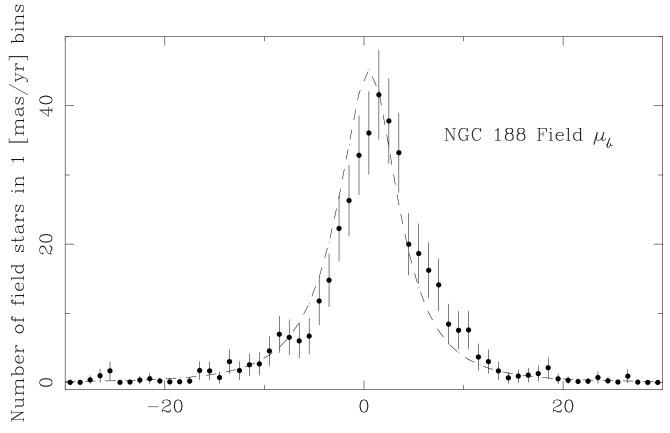




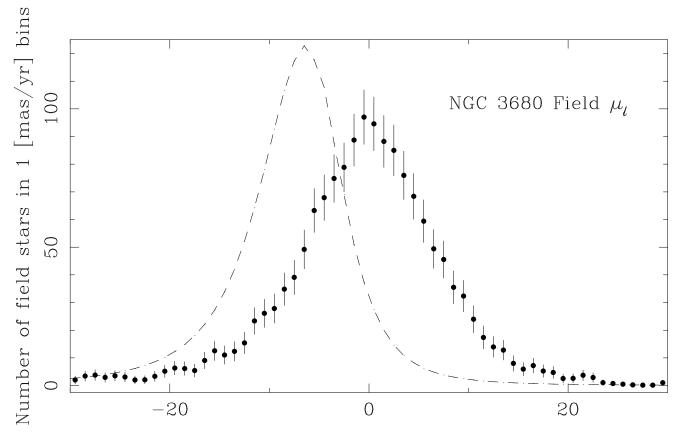




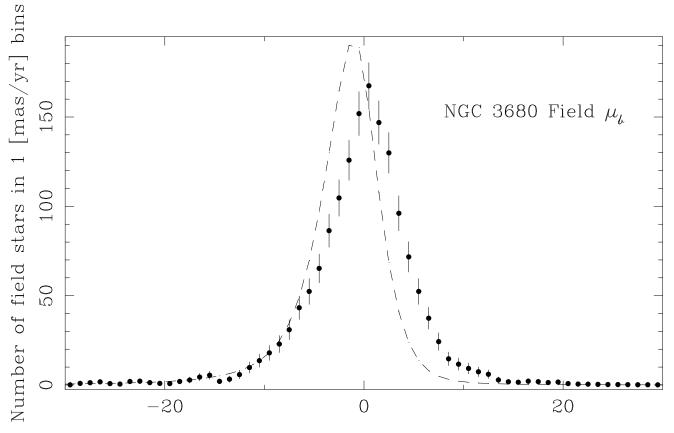
Proper motion in Galactic longitude [mas/yr]



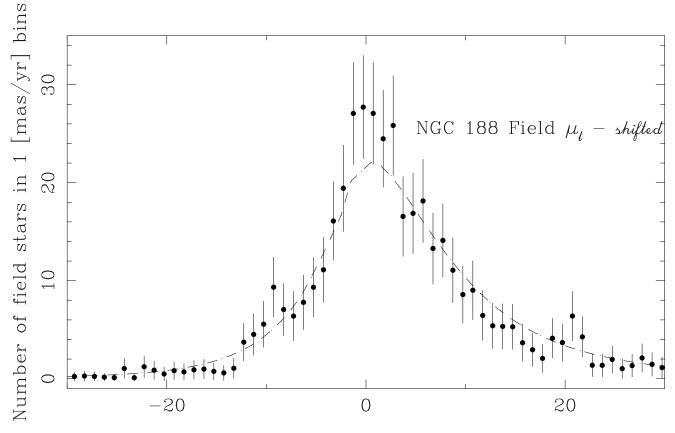
Proper motion in Galactic latitude [mas/yr]



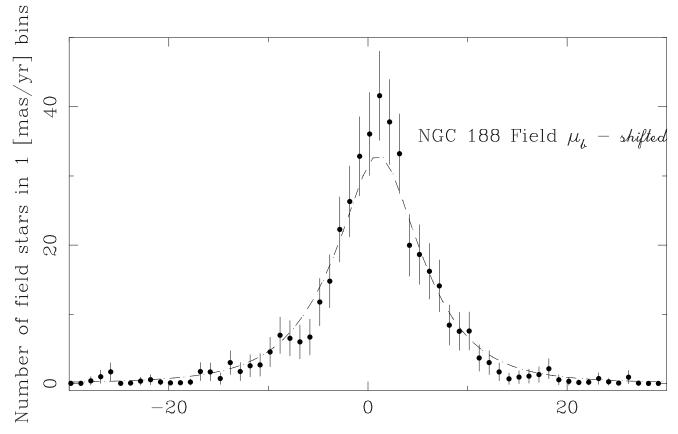
Proper motion in Galactic longitude [mas/yr]



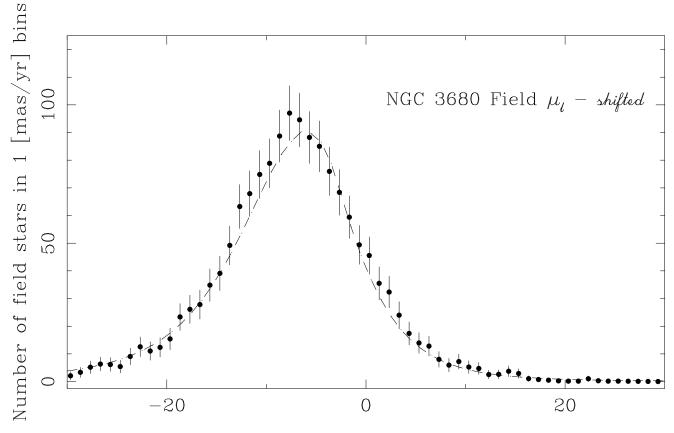
Proper motion in Galactic latitude [mas/yr]



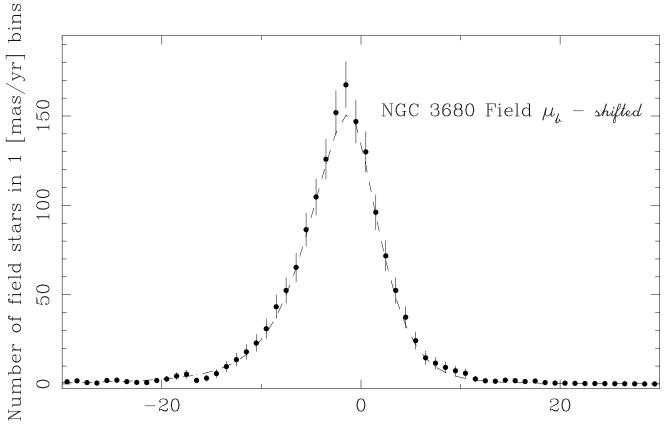
Proper motion in Galactic longitude [mas/yr]



Proper motion in Galactic latitude [mas/yr]



Proper motion in Galactic longitude [mas/yr]



Proper motion in Galactic latitude [mas/yr]